The Astrophysical Journal, 608:935–944, 2004 June 20

THE EFFECTS OF ROTATION ON THERMAL X-RAY AFTERGLOWS RESULTING FROM PULSAR GLITCHES

C. Y. Hui and K. S. Cheng
Department of Physics, University of Hong Kong, Chong Yuet Ming Physics Building, Pokfulam Road, Hong Kong, China; cyhui@graduate.hku.hk, hrspksc@hkucc.hku.hk
Received 2003 December 3; accepted 2004 March 1

ABSTRACT

We derive the anisotropic heat transport equation for rotating neutron stars, and we also derive the thermal equilibrium condition in a relativistic rotating axisymmetric star through a simple variational argument. With a simple model of a neutron star, we model the propagation of heat pulses resulting from transient energy releases inside the star. Such sudden energy release can occur in pulsars during glitches. Even in a slow rotation limit ($\Omega \leq 1 \times 10^3$ s^{-1}), the results with rotational effects involved could be noticeably different from those obtained with a spherically symmetric metric in terms of the timescales and magnitudes of thermal afterglow. We also study the effects of gravitational lensing and frame dragging on the X-ray light curve pulsations. Our results indicate that the effect of rotation on the light-curve modulation is small and that the spacetime-curvature effect predominates. The metric components and rotational deformation of the stellar structure are calculated using Hartle-Thorne formalism. We have applied our model to study the thermal response timescales of pulsars after glitches and find that the centrifugal force produced by rotation can substantially reduce the response time by a factor of 3 between a nonrotating star and a rotating star with $\Omega \sim 900$ s^{-1}. The equation of state can also affect the duration of the response.

Subject headings: dense matter — stars: evolution — stars: interiors — stars: neutron — X-rays: stars

1. INTRODUCTION

Rotation-powered pulsars spin down as they radiate. During the spin-down epoch, some pulsars exhibit dramatic events called "glitches," which are sudden spin-ups of the star. Many observations have identified such phenomena (Krawczyk et al. 2003; Hobbs et al. 2002; Lyne et al. 2000; Wang et al. 2000). Numerous mechanisms have been proposed to explain the origin of pulsar glitches, and the superfluid-driven mechanism (Anderson & Itoh 1975; Alpar et al. 1984) and the starquake mechanism (Ruderman 1969; Baym & Pines 1971) are the most widely accepted. The starquake mechanism is based on the idea that a neutron star possesses a solid crust. As the star spins down, centrifugal force on the crust decreases and gravity pulls the crust to a less oblate equilibrium shape. This change in stellar shape induces stress in the crust. However, the rigidity of the solid crust resists this stress, and the shape remains more oblate than the equilibrium value. When the crust stresses reach a critical value, the crust cracks and the glitch energy is released in a small volume at the weak regions in the solid crust. This localized energy releasing induces an uneven heating of the surface, which corresponds to the "spot" case. It should be noted that the starquake-driven glitches can occur anywhere within the crust where a Coulomb lattice exists.

The superfluid-driven mechanism (Anderson & Itoh 1975) suggests that the spin-up of the crust is produced by transferring angular momentum from a rotating superfluid to the more slowly rotating crust. Apart from spinning up, the mechanism also produces frictional heating and hence local energy dissipation (Alpar et al. 1984; Shibazaki & Lamb 1989). Moreover, the critical angular speed difference for spinning is inversely proportional to the distance from the rotational axis, so this process concerns only equatorial regions and hence a ring structure at the rotational equator is produced (Cheng et al. 1988). It should be noted that superfluid-driven glitches can occur only in the inner crust, where superfluid and Coulomb lattices coexist.

Some other glitch mechanisms have been proposed. For example, Link & Epstein (1996) have proposed a thermal glitch mechanism. In this model, a large increase in the vortex creep rate is induced by a temperature perturbation. As a result, the superfluid quickly loses angular momentum and delivers a spin-up torque to the crust. Carter et al. (2000) have suggested that centrifugal buoyancy forces are the origin of pressure gradients sufficient to crack the crust and allow outward vortex motion.

Several authors (Van Riper et al. 1991; Chong & Cheng 1994; Hirano et al. 1997; Cheng et al. 1998; Tang & Cheng 2001) have suggested that the thermal evolution of a pulsar after glitches would provide a good method to determine the equation of state for neutron stars. The glitch energy was first assumed to be released in a spherical shell at a certain density inside the pulsar (Van Riper et al. 1991; Chong & Cheng 1994; Hirano et al. 1997), although this does not seem realistic. These authors also show that the glitches in the "shell" case cannot produce very significant observed results for young pulsars.

Cheng et al. (1998) argue that if a good fraction of glitch energy is released in a small volume, namely, the spot case, then instead of the heating up the entire stellar surface, even a small fraction of glitch energy can heat up a small area of the stellar surface drastically. This would result in a periodic hard thermal X-ray pulse emission that should stand out clearly from the soft X-ray background. They suggest that by observing the timescales of thermal X-ray afterglows resulting from glitches, the equations of state of neutron stars can be determined. However, the energy transport in the spot case is clearly not spherically symmetric. They derive the general expression of the relativistic thermal transport and energy balance equations without assuming spherical symmetry and use these equations to study the evolution of the hot spot on the surface of the neutron star after glitches.

Tang & Cheng (2001) incorporate the relativistic light bending effect (Pechenick et al. 1983) and magnetic field effect (Page 1995) in their calculations. They show that these effects can significantly affect the intensity and the pulse shape of the transient X-rays resulting from glitches.

Apart from the equation of state, the glitch mechanism also affects the thermal responses. Larson & Link (2002) simulate the emergence of a thermal wave at the stellar surface with two different glitch models and compare the results with the data from *Chandra* observations of thermal emission from the 2000 January glitch in the Vela pulsar (Helfand et al. 2001).

All the aforementioned studies have not considered the effects of the rotating metric, which can affect the timescale, intensity, and pulse shape of the transient X-ray pulses. In studies of the spot case (Cheng et al. 1998; Tang & Cheng 2001), the Schwarzschild metric is used and all the effects of the rotating metric are ignored. For a complete analysis, the development of an anisotropic transport equation is clearly needed, and instead of the Schwarzschild metric a rotating metric must be used.

We organize the paper as follows. In § 2 we review the Hartle-Thorne formalism. In § 3 we study the effects of rotation on thermal equilibrium configuration. In § 4 we describe the development of the anisotropic heat transport equation. In § 5 we describe a Markovian random walk method to simulate the thermal afterglows resulting from glitches. In § 6 we study the effects of gravitational lensing and frame dragging on the X-ray light curves. In § 7 we discuss the physical interpretation of the numerical results.

2. HARTLE-THORNE FORMALISM

The general expression for the line element of an axial symmetric spacetime is determined by time-translational invariance and axial-rotational invariance:

$$ds^2 = e^{2\nu(r,\theta)}dt^2 - e^{2\lambda(r,\theta)}dr^2 - r^2e^{2\psi(r,\theta)}\left\{d\theta^2 + \sin^2\theta[d\phi - \omega(r,\theta)dt]^2\right\}, \quad (1)$$

where we have chosen the units $G = c = 1$.

To calculate the rotating stellar model as a perturbative expansion from a spherical star, we adopt the method proposed by Hartle (1967) and Hartle & Thorne (1968). We calculate the perturbations up to second order of the rotational frequency. The perturbed geometry of spacetime is described by

$$\begin{aligned} ds^2 = {} & e^{2\nu(r)}\{1 + 2[h_0 + h_2P_2(\cos\theta)]\}dt^2 \\ & - \frac{1 + 2[2m_0 + m_2P_2(\cos\theta)]/(r - 2M)}{1 - 2M/r}dr^2 \\ & - r^2[1 + 2(\nu_2 - h_2)P_2(\cos\theta)] \\ & \times \left[d\theta^2 + \sin^2\theta(d\phi - \omega\,dt)^2\right] \\ & + O(\Omega^3), \end{aligned} \quad (2)$$

where Ω is the rotational frequency of the star, $P_2(\cos\theta) = (3\cos^2\theta - 1)/2$ is the Legendre polynomial of the second order, and h_0, h_2, m_0, m_2, and ν_2 are all functions of r that are proportional to Ω^2 (Hartle 1967; Hartle & Thorne 1968). The terms $\nu(r)$ and M are the metric function and the gravitational mass of a nonrotating star, respectively. With the chosen equation of state and the central density, they can be calculated by integrating the set of equations

$$\frac{dP}{dr} = -(\rho + P)\frac{M + 4\pi r^3}{r(r - 2M)}, \quad (3)$$

$$\frac{dM}{dr} = 4\pi r^2\rho, \quad (4)$$

$$\frac{d\nu}{dr} = -\frac{dP}{dr}(\rho + P)^{-1} \quad (5)$$

outward from the center with the boundary conditions $M(0) = 0$, $P(R) = 0$, and $\nu(R) = \frac{1}{2}\ln[1 - 2M(R)/R]$, where R is the radius of the nonrotating star. For a uniformly and rigidly rotating star, the contravariant components of the four-velocity are

$$u^t = e^{-\nu}\left[1 + \frac{1}{2}r^2\sin^2\theta\bar{\omega}^2e^{-2\nu} - h_0 - h_2P_2(\cos\theta)\right], \quad (6)$$

$$u^\phi = \Omega u^t, \quad (7)$$

$$u^r = u^\theta = 0, \quad (8)$$

where $\bar{\omega} = \Omega - \omega$ and ω defines the dragging frequency of local inertial frames.

The star is centrifugally deformed by rotation. In the reference frame that is momentarily moving with the fluid, the energy-density distribution including the effect of rotation is

$$\rho + \Delta\rho = \rho + (\rho + P)\left[p_0^* + p_2^*P_2(\cos\theta)\right]\frac{d\rho}{dP}. \quad (9)$$

All the necessary rotational perturbation functions are calculated from the equations described below.

The angular velocity of the fluid relative to the local inertial frame $\bar{\omega}$ is found by integrating the differential equation

$$\frac{1}{r^4}\frac{d}{dr}\left(r^4j\frac{d\bar{\omega}}{dr}\right) + \frac{4}{r}\frac{dj}{dr}\bar{\omega} = 0, \quad (10)$$

where

$$j(r) = e^{-\nu}\left(1 - \frac{2M}{r}\right)^{1/2}. \quad (11)$$

This equation can be integrated outward from the center of the star with the boundary conditions $\bar{\omega} = \bar{\omega}_c$ and $d\bar{\omega}/dr = 0$. The constant $\bar{\omega}_c$ is chosen arbitrarily. When the surface is reached, one can determine the angular momentum $J = \frac{1}{6}R^4(d\bar{\omega}/dr)_{r=R}$, as well as the angular velocity $\Omega = \bar{\omega}(R) + 2J/R^3$, corresponding to the chosen $\bar{\omega}_c$.

The terms p_0^* and m_0 can be calculated by integrating the equations

$$\frac{dm_0}{dr} = 4\pi r^2\frac{d\rho}{dP}(\rho + P)p_0^* + \frac{1}{12}j^2r^4\left(\frac{d\bar{\omega}}{dr}\right)^2 - \frac{1}{3}r^3\frac{dj^2}{dr}\bar{\omega}^2, \quad (12)$$

$$\frac{dp_0^*}{dr} = -\frac{m_0(1 + 8\pi r^2P)}{(r - 2M)^2} - \frac{4\pi(\rho + P)r^2}{(r - 2M)}p_0^* + \frac{1}{12}\frac{r^4j^2}{(r - 2M)}\left(\frac{d\bar{\omega}}{dr}\right)^2 + \frac{1}{3}\frac{d}{dr}\left(\frac{r^3j^2\bar{\omega}^2}{r - 2M}\right) \quad (13)$$

outward from the center with the boundary condition $p_0^* = m_0 = 0$. Owing to the centrifugal force, a rotating star will have a larger mass than a nonrotating one for a given central density. The increment is given as $\Delta M = m_0(R) + J^2/R^3$, and h_0 can be obtained from the algebraic relations. Inside the star,

$$h_0 = -p_0^* + \frac{1}{3} r^2 e^{-2\nu} \bar{\omega}^2 + h_{0c}, \tag{14}$$

outside the star,

$$h_0 = -\frac{\Delta M}{r - 2M} + \frac{J^2}{r^3(r - 2M)}, \tag{15}$$

and h_{0c} is a constant determined by demanding that h_0 be continuous across the surface.

The remaining four perturbation functions (ν_2, h_2, m_2, and p_2^*) can be calculated from the following equations:

$$\frac{d\nu_2}{dr} = -2\frac{d\nu}{dr} h_2 + \left(\frac{1}{r} + \frac{d\nu}{dr}\right)\left[-\frac{1}{3} r^3 \frac{dj^2}{dr} \bar{\omega}^2 + \frac{1}{6} j^2 r^4 \left(\frac{d\bar{\omega}}{dr}\right)^2\right], \tag{16}$$

$$\begin{aligned}\frac{dh_2}{dr} = &\left\{-2\frac{d\nu}{dr} + \frac{2r}{r - 2M}\left(\frac{d\nu}{dr}\right)^{-1}\left[2\pi(\rho + P) - \frac{M}{r^3}\right]\right\} h_2 \\ &- \frac{2\nu_2}{r(r - 2M)}\left(\frac{d\nu}{dr}\right)^{-1} \\ &+ \frac{1}{6}\left[\frac{d\nu}{dr} r - \frac{1}{2(r - 2M)}\left(\frac{d\nu}{dr}\right)^{-1}\right] r^3 j^2 \left(\frac{d\bar{\omega}}{dr}\right)^2 \\ &- \frac{2}{3}\left[\frac{d\nu}{dr} r + \frac{1}{2(r - 2M)}\left(\frac{d\nu}{dr}\right)^{-1}\right] r^2 \bar{\omega}^2 j \frac{dj}{dr},\end{aligned} \tag{17}$$

$$m_2 = (r - 2M)\left[-h_2 - \frac{1}{3} r^3 \left(\frac{dj^2}{dr}\right)\bar{\omega}^2 + \frac{1}{6} r^4 j^2 \left(\frac{d\bar{\omega}}{dr}\right)^2\right], \tag{18}$$

$$p_2^* = -h_2 - \frac{1}{3} r^2 e^{-\nu} \bar{\omega}, \tag{19}$$

with boundary conditions $\nu_2 = 0$ and $h_2 = 0$ at the origin.

3. THERMAL EQUILIBRIUM CONFIGURATION

Consider a particle in the star with energy E. The energy of this particle as measured by a distant observer, E_∞, can be related to its locally measured value E by $E_\infty = E/u^t$. Next, we consider the energy transport from one region to another in an isolated star without any change in the density of particles. For a local observer, the fundamental thermodynamics relation $dE = T\,dS$ is always valid, where dS is the change in entropy per baryon and T is the locally measured temperature.

By following the scheme of Zel'dovich & Novikov (1971), the equilibrium condition can be obtained by extremizing the entropy of the system with the constraint that the total energy is conserved:

$$\begin{aligned}\delta\left(\int Sn\,dV + \Lambda \int E_\infty n\,dV\right) &= 0, \\ \int \left(\delta S + \Lambda \frac{\delta E}{u^t}\right) n\,dV &= 0, \\ \int \left(1 + \Lambda \frac{T}{u^t}\right) n\,dV &= 0,\end{aligned} \tag{20}$$

where n is baryon number density, dV is proper volume element, and Λ is a Lagrange multiplier. Consequently, the thermal equilibrium condition of a relativistic axisymmetric star is formulated as

$$\frac{T}{u^t} = \Lambda^{-1} = \text{constant}. \tag{21}$$

This result, which is obtained from a relatively simple variation argument, is consistent with the one derived more vigorously by Miralles et al. (1993). Also, there is an underlying assumption that the neutron star is in rigid rotation. If it were not, the internal friction would produce heat and our variational argument would no longer be valid.

The aforementioned isothermal approximation is only appropriate in the interior. There is a thin atmosphere surrounding the isothermal core that sustains an appreciable temperature gradient. For spherically symmetric cases, model atmospheres have already been calculated by Gudmundsson et al. (1983) that give the surface temperature T_s as a function of the temperature at the base of the atmosphere T_b and the surface gravity g_s. The base of the atmosphere is chosen at a particular density ρ_b. For our study, it is chosen at $\rho_b = 10^{10}$ g cm^{-3}:

$$T_{b_9} = 0.1288\left(\frac{T_{s_6}^4}{g_{s_{14}}}\right)^{0.455}. \tag{22}$$

We shall assume that this relation is valid in the slow-rotation case with a suitable choice of an effective local surface gravity $g_s(\theta)$ that takes the centrifugal deformation into account. Consequently, the surface temperature $T_s(T_b, \theta)$ depends on the polar angle.

4. GENERAL RELATIVISTIC ANISOTROPIC HEAT TRANSPORT EQUATION

With an intention to model the most general case of energy transport inside a rotating neutron star, we derive the heat transport equation without making the assumption of spherical symmetry in energy transport, stellar structure, or spacetime.

To derive the equation, we assume that there are no other entropy-generating mechanisms besides diffusion and fluid motion inside the star, because of the thermal effects being negligible. The energy-momentum tensor inside a star consists of a perfect fluid, which allows the heat flow to be written as $T^{\mu\nu} = (\rho + P)u^\mu u^\nu - P g^{\mu\nu} + u^\mu q^\nu + u^\nu q^\mu$, where $g^{\mu\nu}$ denotes the inverse components of equation (1), u^μ is the four-velocity of the fluid flow, which has been described in § 2, and ρ and P are the total energy density and pressure measured in the rest frame of the fluid (Tolman 1934). The heat flow is given by $q^\alpha = K(g^{\alpha\beta} - u^\alpha u^\beta)(T_{;\beta} - T a_\beta)$, where $a_\alpha = u_{\alpha;\beta} u^\beta$ is the four-acceleration and K is the thermal conductivity (Tolman 1934).

No matter how complicated the transport equation is, the basic principle is that the underlying physics is nothing but the law of conservation of energy. In relativity, the energy-momentum tensor embodies a compact description of energy and momentum. To be more specific, the transport equation can be derived by the conservation of the energy-momentum tensor, namely,

$$T^{t\alpha}_{\ ;\alpha} = T^{tt}_{\ ;t} + T^{tr}_{\ ;r} + T^{t\theta}_{\ ;\theta} + T^{t\phi}_{\ ;\phi} = 0, \tag{23}$$

where

$$T^{tt}_{;t} = \left[u^t u^t + (u^t u^t - g^{tt}) \frac{dP}{d\rho} \right] \frac{\partial \rho}{\partial t} + 2u^t K \left[(g^{tt} - u^t u^t) \frac{\partial^2 T}{\partial t^2} + \left(g^{t\phi} - u^t u^\phi \right) \frac{\partial^2 T}{\partial t \partial \phi} \right] + 2\Gamma^t_{rt} f^r + 2\Gamma^t_{\theta t} f^\theta, \quad (24)$$

$$T^{tr}_{;r} = \frac{\partial f^r}{\partial r} + \frac{\partial \lambda}{\partial r} f^r + \frac{\partial \lambda}{\partial \theta} f^\theta + \Gamma^t_{tr} f^r + \Gamma^t_{r\phi} u^\phi q^r, \quad (25)$$

$$T^{t\theta}_{;\theta} = \frac{\partial f^\theta}{\partial \theta} + \Gamma^t_{t\theta} f^\theta + \Gamma^\theta_{r\theta} f^r + \Gamma^\theta_{\theta\theta} f^\theta + \Gamma^t_{\theta\phi} u^\phi q^\theta, \quad (26)$$

$$T^{t\phi}_{;\phi} = \frac{\partial f^\phi}{\partial \phi} + \Gamma^\phi_{\theta\phi} f^\theta + \Gamma^\phi_{r\phi} f^r + \Gamma^t_{\theta\phi} u^\phi q^\theta + \Gamma^t_{r\phi} u^\phi q^r, \quad (27)$$

where $f^i = T^{ti}$ is the energy flow per unit area parallel to the i-direction. $\Gamma^\gamma_{\alpha\beta}$ are the Christoffel symbols, and $\partial\rho/\partial t$ in $T^{tt}_{;t}$ is the rate of change of energy density measured by distant observer, which can be expressed in the locally measured quantity, namely, $\partial\rho/\partial\tau$. It depends on the processes under consideration. If only heat conduction and neutrino emission are considered, we have $\partial\rho/\partial\tau = C_v(\partial T/\partial\tau) + Q_\nu$, where C_v and Q_ν are the heat capacity and the neutrino emissivity measured in the local frame, respectively. Expressing this in the coordinate time t, we have $\partial\rho/\partial t = C_v(\partial T/\partial t) + (Q_\nu/u^t)$. Using this relation and equation (23), we obtain the heat diffusion equation:

$$0 = \left[u^t u^t + (u^t u^t - g^{tt}) \frac{dP}{d\rho} \right] \left(C_v \frac{\partial T}{\partial t} + \frac{Q_\nu}{u^t} \right) + 2u^t K \left[(g^{tt} - u^t u^t) \frac{\partial^2 T}{\partial t^2} + \left(g^{t\phi} - u^t u^\phi \right) \frac{\partial^2 T}{\partial t \partial \phi} \right] + \frac{\partial f^r}{\partial r} + \frac{\partial f^\theta}{\partial \theta} + \frac{\partial f^\phi}{\partial \phi} + \left(3\Gamma^t_{rt} + \frac{\partial \lambda}{\partial r} + \Gamma^\theta_{r\theta} + \Gamma^\phi_{r\phi} \right) f^r + \left(3\Gamma^t_{t\theta} + \frac{\partial \lambda}{\partial \theta} + \Gamma^\theta_{\theta\theta} + \Gamma^\phi_{\theta\phi} \right) f^\theta + 2\Gamma^t_{r\phi} u^\phi q^r + 2\Gamma^t_{\theta\phi} u^\phi q^\theta. \quad (28)$$

In the nonrotational limit, the spacetime is described by the diagonal Schwarzschild metric, and the above equation recovers the case obtained by Cheng et al. (1998). It should also be noted that this equation recovers the well-known Newtonian case.

5. SIMULATIONS OF THERMAL AFTERGLOWS THAT RESULT FROM GLITCHES

The anisotropic relativistic heat transport equation, i.e., equation (28), can be rearranged into a single-variable partial differential equation (see the Appendix). We employ a quantized Monte Carlo technique for the simulation of heat transport inside a rotating neutron star. Dynamic stochastic processes are simulated by using rate coefficients (i.e., diffusion coefficient D, drift coefficient v, annihilation coefficient μ, and local depletion S). These coefficients are determined by rearranging the rate equation (28). In order to perform the simulations, some assumptions must be made. First, we assume that the quantities D_i, v_i, and μ_i depend only on position, where i denotes the motion of energy carriers in r, θ, and ϕ. Much more general dependences result in nonlinear behavior. Second, if the grid sizes are fine enough, the energy carriers transit from the surrounding grid points in the previous time step with equal probability. Third, we neglect the thermal effects on the stellar structure.

There are two terms of mixed derivative and second time derivative present in the equation. There is no easy way to incorporate these in a random walk approach. However, their coefficients contain only the factors of $(g^{tt} - u^t u^t)$ and $(g^{t\phi} - u^t u^\phi)$. Since the zero-order terms are canceled in the subtractions, only the second-order perturbation terms remain. Up to the highest rotational frequency that we have considered (1×10^3 s^{-1}), these coefficients are still negligible in comparison with the smallest term that we have taken into account, so it is safe to drop them in the simulations.

With these assumptions, the heat transport inside a rotating neutron star can now be simulated by a straightforward Markovian random walk (MacKeown 1997): (1) Specify the initial condition $T(\boldsymbol{r}, 0)$ and quantize it by a large number M of "walkers" whose starting positions are selected in accordance with $T(\boldsymbol{r}, 0)$ and whose random walk is modeled. (2) In each time step Δt, a weight is attached to each walker according to the survival probability $\mu\Delta t$ by means of "survival biasing" (MacKeown 1997). Then it is displaced by $\Delta x_i = \pm(2D_i\Delta t)^{1/2} + v_i\Delta t$ in each degree of freedom, where the sign of the step is chosen with equal probability on the basis of a uniform random variate. (3) Incorporate the local depletion $S\Delta t$. (4) Repeat steps 2 and 3 M times for each walker. (5) Repeat step 4 N times. (6) Plot the distribution of the walkers, and this should approximate the solution $T(\boldsymbol{r}, t)$ at $t = N\Delta t$. Note that the finite value of walkers M introduces an unavoidable statistical fluctuation. Also, the finite time step used will introduce a truncation error.

Since we intend to investigate the effect of rotation on the heat transport, we adopt a simple model of a neutron star. We employ the method described in § 2 to calculate the rotational stellar structure. The stellar structure is determined by the equation of state. We use the equation of state of neutron matter from Pandharipande (1971) in our calculation. We have considered the contribution of protons, neutrons, and electrons to the heat capacity (Maxwell 1979), but the most important term is the contribution of electrons. We consider only the neutrino emissivities due to neutron-neutron bremsstrahlung, proton-neutron bremsstrahlung, and the modified Urca process (Maxwell 1979). We adopt the analytic formulae of thermal conductivity presented by Flowers & Itoh (1981).

We calculate temperature distributions for a "ring" case and a "spot" case. For both cases, heat inputs are deposited at the depth of the crust where $\rho \sim 10^{13}$ g cm^{-3}. The ratio $R/M \sim 8$ corresponds to $M \sim 1\ M_\odot$ and $R \sim 10$ km. The core temperature is taken to be 10^7 K. With $\Delta E = 10^{42}$ ergs deposited around the equator (i.e., $\theta = 90^\circ$), Figure 1 illustrates the polar angular surface temperature distribution of a rotational ring case with $\Omega = 7.6 \times 10^2$ s^{-1}. For the spot case, we choose $\Delta E = 10^{42}$ ergs to be released at $\theta = \phi = 90^\circ$. Figure 2 illustrates the azimuthal profile of surface temperature at the rotational equator of the hot spot for a rotational case with $\Omega = 7.6 \times 10^2$ s^{-1}. Figure 3 illustrates the evolution of the thermal X-ray flux of the spot case. Three cases with different rotational frequency are compared. With the mass increased by ~33% and the radius decreased by ~1%, the R/M ratio is reduced to ~6, which indicates that the gravitational effect is enhanced. We recalculate the spot case with this R/M ratio, and the results for three cases with different rotational frequency are shown in Figure 4. The timescale and

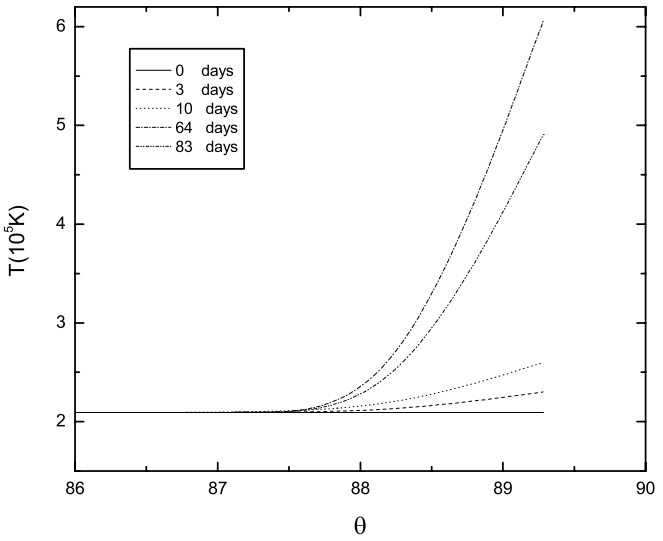

FIG. 1.—Surface temperature of a ring case as a function of polar angle for a neutron star with $R/M \sim 8$, $\Omega = 7.6 \times 10^2$ s^{-1}, $T_c = 10^7$ K, and $\Delta E = 10^{42}$ ergs at $\rho_{\rm glitch} = 10^{13}$ g cm^{-3} and $\theta = 90^\circ$. The inset denotes days elapsed after the heat deposition.

the magnitude of the afterglows for the nonrotational cases are consistent with those obtained by previous authors (Tang & Cheng 2001).

The heat propagation time τ is approximately inversely proportional to the diffusion coefficient D_r, which is proportional to thermal conductivity K and inversely proportional to heat capacity C_v. In the region that we are interested in, the heat capacity is proportional to temperature while the thermal conductivity is inversely proportional to the temperature. Hence, τ is roughly proportional to the temperature squared. It can be seen that heat propagation becomes much slower as the temperature becomes higher. For this reason, the duration of the afterglow for the ring case is shorter than that for the spot case for the same heat input. Comparing the nonrotational flux curve of the spot case with $R/M \sim 8$ in Figure 3 and that with $R/M \sim 6$ in Figure 4, we find that the afterglow takes a longer time in the model with $R/M \sim 6$ because of a larger mass

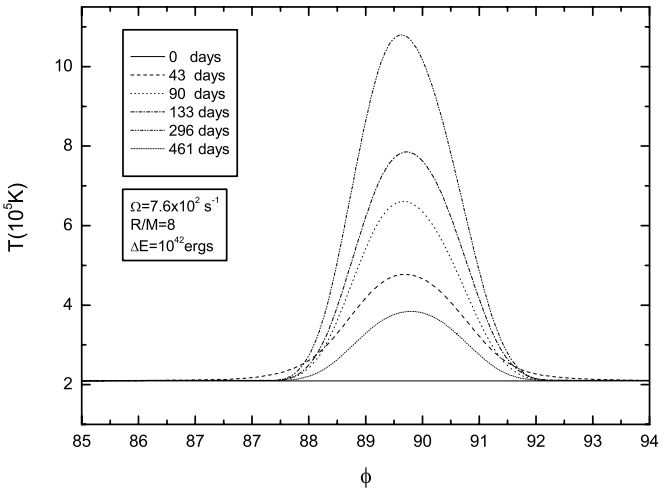

FIG. 2.—Surface temperature of a spot case at the equator as a function of azimuthal angle for a neutron star with $R/M \sim 8$, $\Omega = 7.6 \times 10^2$ s^{-1}, $T_c = 10^7$ K, and $\Delta E = 10^{42}$ ergs at $\rho_{\rm glitch} = 10^{13}$ g cm^{-3} and $\theta = \phi = 90^\circ$. The inset denotes days elapsed after the heat deposition.

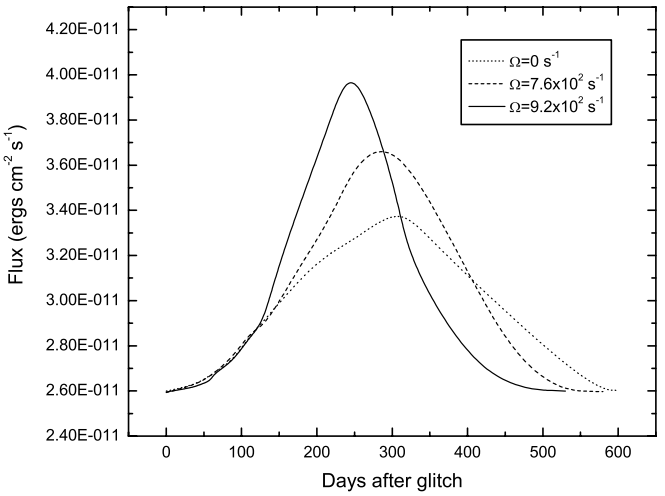

FIG. 3.—Evolution curves of thermal X-ray flux for a neutron star with $R/M \sim 8$, $T_c = 10^7$ K, and $\Delta E = 10^{42}$ ergs at $\rho_{\rm glitch} = 10^{13}$ g cm^{-3} and $\theta = \phi = 90^\circ$ for a spot case. Three cases with different rotational frequency are compared.

underneath the location of the energy release, which hinders the propagation of the heat pulse to the surface. Comparing the rotational cases with the nonrotational ones in Figures 3 and 4, we find that the duration of the thermal afterglow is shortened when the effect of rotation is introduced. To further investigate this effect, we carry out more simulations of the spot case with different rotational frequencies. Figure 5 illustrates the fractional decrease in the duration of the thermal afterglow as a function of rotational frequency for $R/M \sim 8$ and $R/M \sim 6$.

The rotational effects can originate from the centrifugal forces in rotating neutron stars. When the energy ΔE is released in a localized region at the equator, it can be viewed as an equivalent mass $\sim \Delta E/c^2$ that corotates with the star. This leads to a natural interpretation that centrifugal forces prompt a faster and larger thermal response. In Figure 5 it should be noted that the fractional decrease in the duration is larger in the case of $R/M \sim 6$ than that in the case of $R/M \sim 8$ for a given Ω. This indicates the other effect of rotation on the heat transfer. Apart from prompting a faster heat propagation, centrifugal forces also deform the star. As pointed out by some

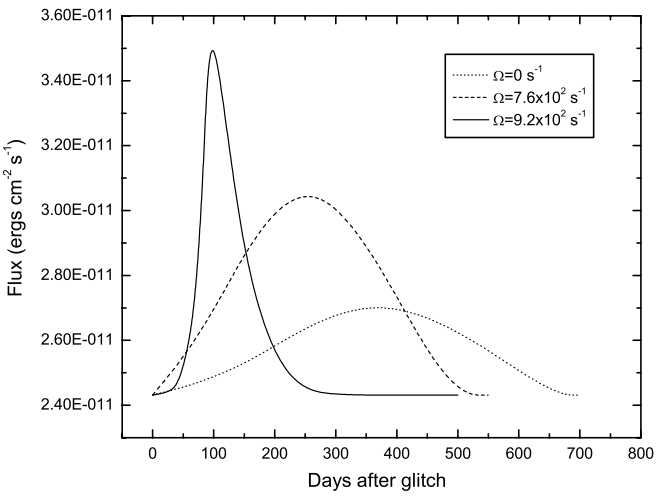

FIG. 4.—Same as Fig. 3, but with $R/M \sim 6$.

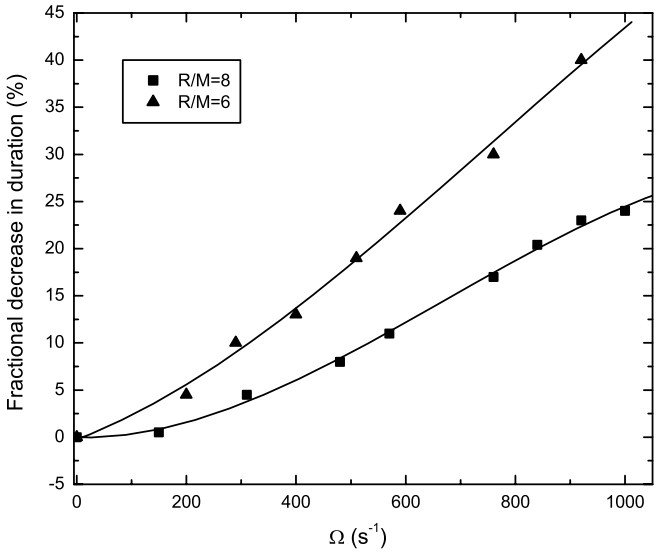

FIG. 5.—Fractional decrease in the duration of thermal afterglow of a spot case as a function of rotational frequency for $R/M \sim 8$ and $R/M \sim 6$.

ellipticity studies (Abramowicz 1990; Chandrasekhar & Miller 1974), the denser a neutron star, the less eccentric it is. A star with $R/M \sim 8$ is more eccentric than one with $R/M \sim 6$. Since the heat inputs are deposited at the depth where $\rho \sim 10^{13}$ g cm^{-3} at the equator in both models, the heat pulse needs to propagate through a larger distance in a more eccentric star in order to reach the surface and give the afterglow.

Nevertheless, the behavior of centrifugal forces in general relativity is fundamentally different from that in Newtonian physics (Freire & da Costa 1999; Abramowicz et al. 1988, 1993; Abramowicz & Prasanna 1990). One of the questions behind our interpretation is whether there can be inversion of centrifugal forces inside neutron stars. Freire & da Costa (1999) show that most realistic equations of state do not allow the existence of such inversion. Without the bother of centrifugal force inversion, we suggest that rotation introduces two effects on the thermal afterglow. First, it prompts a faster and larger thermal response. Second, it increases the distance that heat needs to travel in order to give an afterglow on the surface. The resultant effect on the duration and the magnitude of the thermal afterglow depends on the interplay between these two factors.

6. THERMAL X-RAY LIGHT CURVES

For the spot case, the locally released energy would modulate the X-ray pulse shape by heating a portion of crust so that more thermal X-rays are emitted at a particular phase. The modulation of X-ray pulse will last until the surface temperature has equilibrated. We now investigate the effects of spacetime curvature and rotation on the thermal X-ray profile.

6.1. *Gravitational Lensing Effect*

Since the surface gravity of a neutron star is tremendous, the effect of gravity on the trajectory of emitted photons must be taken into account. In this section, we choose our coordinates so that the observer is on the positive z-axis at $r = r_0$, where $r_0 \to \infty$ (see Fig. 6). The following scheme of calculating the X-ray light curves resulting from light bending is adapted from Pechenick et al. (1983). The surface of the star is described by angular spherical coordinates θ and ϕ, where θ is measured from the z-axis that we have just defined. When

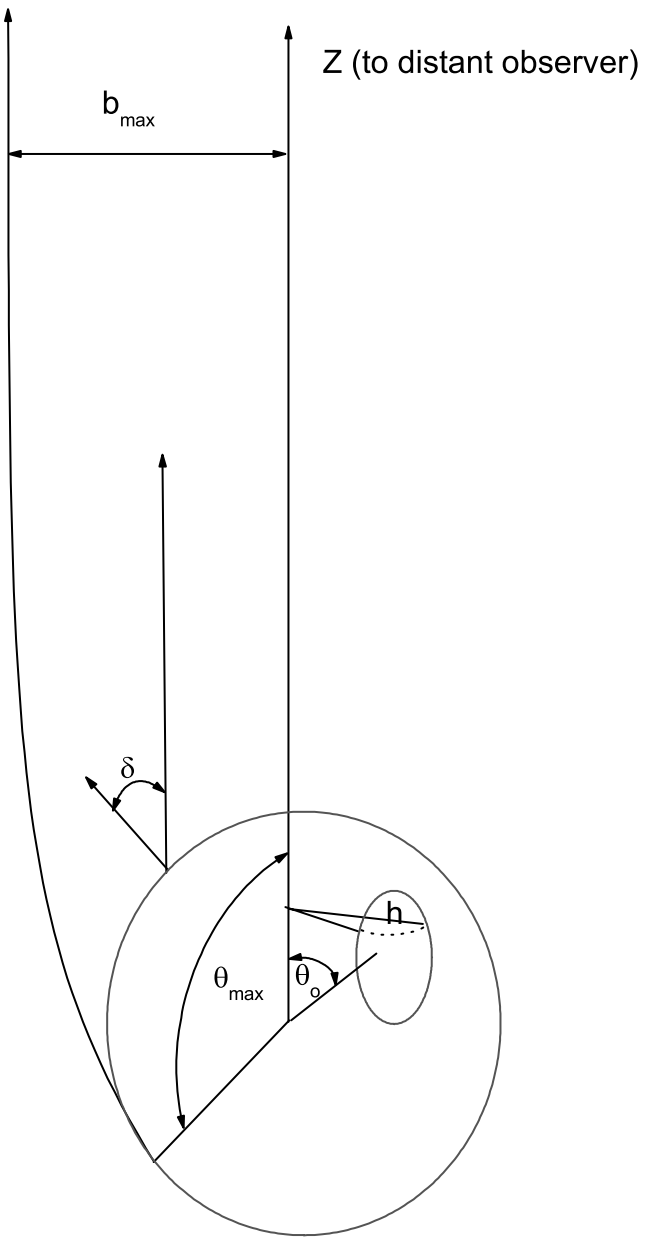

FIG. 6.—Geometry used to determine the brightness of a hot spot.

the photon is being emitted from the surface at an angle δ, as illustrated in Figure 6, it will be deflected by the gravitational field. It will seem to the observer that it is emitted at angle θ' from the z-axis. Hence, θ is a function of θ':

$$\theta = \int_0^{M/R} \left[\left(\frac{M}{b} \right)^2 - (1 - 2u)u^2 \right]^{-1/2} du, \qquad (29)$$

where $b = r_0\theta'$ and $u = M/r$; b is the impact parameter of the photon.

If the star has the ratio $R/M > 3$, then a photon emitted from the surface and reaching the observer must have an impact parameter $b \le b_{\max}$, where $b_{\max} = R(1 - 2M/R)^{-1/2}$. The maximum possible value of θ occurs when $b = b_{\max}$. We consider a hot spot of angular radius α centered at $\theta = \theta_0$. A function $h(\theta; \alpha, \theta_0)$ is then defined as the range of ϕ included in the "one-dimensional slice" at θ of the hot spot. If

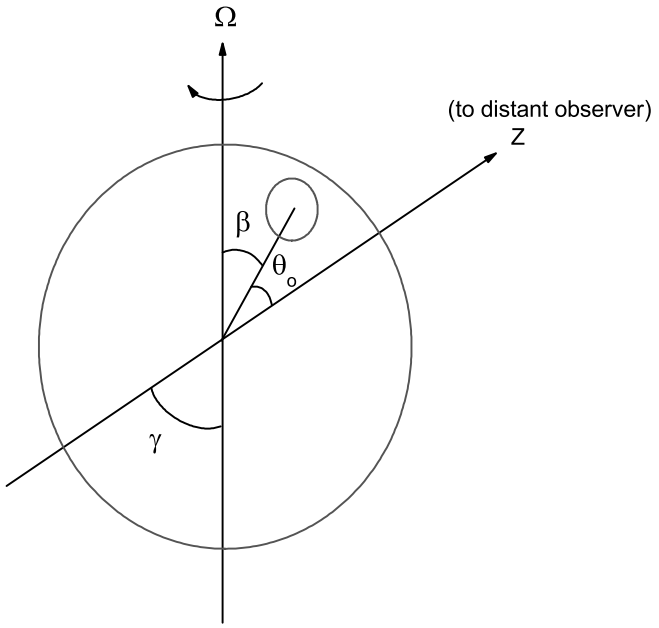

FIG. 7.—Relation of the orientation of the hot spot and the axis of rotation to the observer's line of sight.

$\theta_0 + \alpha \leq \theta_{\max} \leq 180^\circ$ and $\theta_0 - \alpha \geq 0$, then $h(\theta; \alpha, \theta_0)$ is defined as

$$h(\theta;\alpha,\theta_0) = \begin{cases} 2\cos^{-1}\left(\dfrac{\cos\alpha - \cos\theta_0\cos\theta}{\sin\theta_0\sin\theta}\right) & \theta_0 - \alpha \leq \theta \leq \theta_0 + \alpha, \\ 0 & \theta \text{ outside the range } \theta_0 \pm \alpha. \end{cases} \quad (30)$$

When the requirement that the photons under consideration must reach the observer is imposed [not all the photons emitted at (θ, ϕ) can reach the observer], δ is also a function of θ'. Let $x = b/M$ and $x_{\max} = b_{\max}/M$. Then we have

$$\delta = \sin^{-1}\left(\frac{x}{x_{\max}}\right). \quad (31)$$

We will come back to this requirement when we discuss the rotational effect on the pulse shape.

In order to obtain light curves, θ_0 has to be obtained as a function of time. If β is the angle between the axis of rotation of the star and the line joining the center of the hot spot and the center of the star, and γ is the angle between the axis of rotation and the z-axis (see Fig. 7), then

$$\cos\theta_0 = \sin(\beta)\sin(\gamma)\cos(\Omega t) + \cos(\beta)\cos(\gamma), \quad (32)$$

where Ω is the rotational frequency of the star. We are now able to calculate the relative brightness:

$$A\left(\theta_0; f, \frac{M}{R}, \alpha\right) = \left(1 - \frac{2M}{R}\right)^2 \left(\frac{M}{R}\right)^2 \times \int_0^{x_{\max}} f[\delta(x)] h(x;\alpha,\theta_0) x\, dx, \quad (33)$$

where $f(\delta) = 1$ for isotropic emission, $f(\delta) = \cos\delta$ for enhanced emission, and $f(\delta) = \sin\delta$ for suppressed emission. The relationship between A and Ωt is plotted in Figure 8.

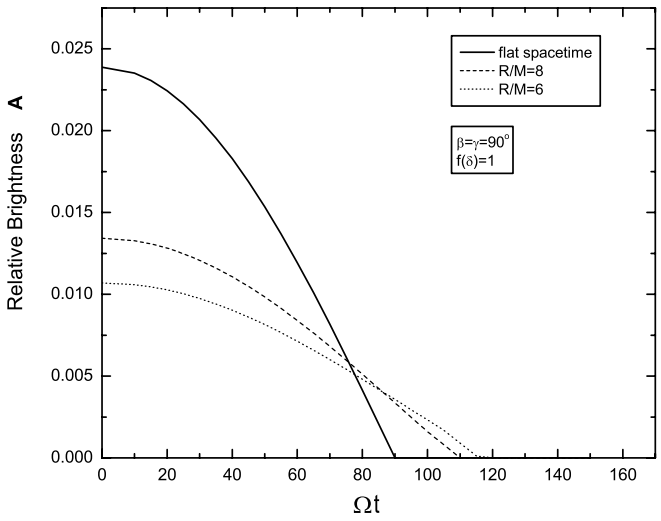

FIG. 8.—Relative brightness A as a function of phase for $\alpha = 5^\circ$, with $f(\delta) = 1$ and $\beta = \gamma = 90^\circ$.

6.2. *Rotational Effect*

Apart from getting bent due to spacetime curvature, the trajectory of a photon emitted in a general direction from a point r_e will be dragged away from its original direction of emission when the rotation of the relativistic star is taken into consideration (Kapoor & Datta 1985). In this section, the axis of rotation is taken to be the z-axis. The net angle of deflection in the trajectory will be given by

$$-\phi_0 = \int_{r_e}^{r_0} \frac{\omega(1+\omega q_e) - q_e e^{2\nu} - e^{2\psi}}{e^{\nu-\lambda}\left[(1+\omega q_e)^2 - q_e^2 e^{2\nu} - e^{2\psi}\right]^{1/2}} dr, \quad (34)$$

with r_e and r_0 denoting the point of emission and the observer's location, respectively; e^ν, e^ψ, and e^λ are the exterior rotating metric components:

$$e^{2\nu} = e^{-2\lambda} = 1 - \frac{2M}{r} + \frac{2J^2}{r^4}, \quad (35)$$

$$e^{2\psi} = r^2 \sin^2\theta. \quad (36)$$

The dragging frequency ω has an analytic exterior solution:

$$\omega(r) = \frac{2J}{r^3}. \quad (37)$$

The term q_e in the integrand of equation (34) is defined as the impact parameter of the photon with rotation taken into consideration:

$$q_e = \left.\frac{e^{\psi-\nu}\left[e^{\psi-\nu}(\Omega-\omega) + \sin\delta\right]}{1 + e^{\psi-\nu}\left[e^{\psi-\nu}\omega(\Omega-\omega) + \Omega\sin\delta\right]}\right|_{r=r_e}. \quad (38)$$

In our case, the source (hot spot) is located at the rotational equator; δ represents the azimuthal angle at which the photon is emitted with respect to the normal vector of the surface as seen in the local rest frame of the star. We choose the convention that $\delta = 0$ for a radial outgoing photon, $\delta < 0$ for a

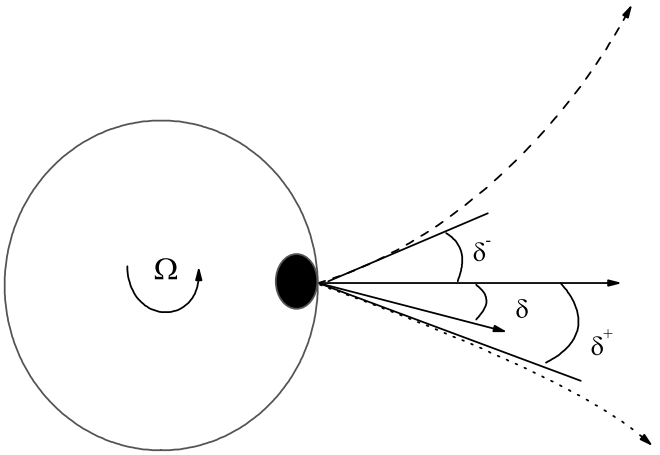

FIG. 9.—Schematic illustration of the effect of frame dragging on the photon trajectory.

tangentially forward photon, and $\delta > 0$ for a tangentially backward photon.

As mentioned in § 6.2, only the photons emitted at a particular value of δ would be received by the distant observer. The value of q_e has been obtained by imposing this requirement. Because of the effect of frame dragging around the neutron star, the situation will be different from that in previous section.

It should be noted that the impact parameter q_e is not symmetric in $\pm\delta$. In principle, this asymmetry will manifest itself in the final pulse shape:

$$\delta_{\rm new} = \delta + \phi_0(\delta). \tag{39}$$

Figure 9 schematically illustrates the deflection of a photon trajectory. As a consequence of rotation, $|\phi_0(\delta)| \neq |\phi_0(-\delta)|$.

This asymmetry does not occur in spherically symmetric spacetime, where however the spacetime curvature will still deflect the trajectory of photon. This can be easily seen if one approximates the corresponding Schwarzschild expression of equation (34) as follows:

$$\phi_0^{\rm S} \approx -\frac{q^{\rm S}}{R}\left[1+\frac{\sin^2\delta\left(2R-3R^{\rm S}\right)}{12(R-2R^{\rm S})}\right], \tag{40}$$

where the superscript "S" refers to the Schwarzschild case. Here $\theta = 90^\circ$ for reasons of symmetry; $R^{\rm S}$ denotes the Schwarzschild radius, and $q^{\rm S} = (e^{\psi-\nu}\sin\delta)_{r=R}$. It can be seen that $|\phi_0^{\rm S}(\delta)| = |\phi_0^{\rm S}(-\delta)|$.

We define the corresponding $\delta_{\rm new}^{\rm S}$ of equation (39) as

$$\delta_{\rm new}^{\rm S} = \delta + \phi_0^{\rm S}(\delta); \tag{41}$$

comparison between $\delta_{\rm new}^{\rm S}$ and $\delta_{\rm new}$ is made in Figure 10. Even in the fastest rotational case that we have considered ($\Omega = 1\times10^3$ s^{-1}) with a relatively small gravitational effect ($R/M \sim 8$), the comparison indicates that the effect of rotation is small and that the effect of spacetime curvature predominates.

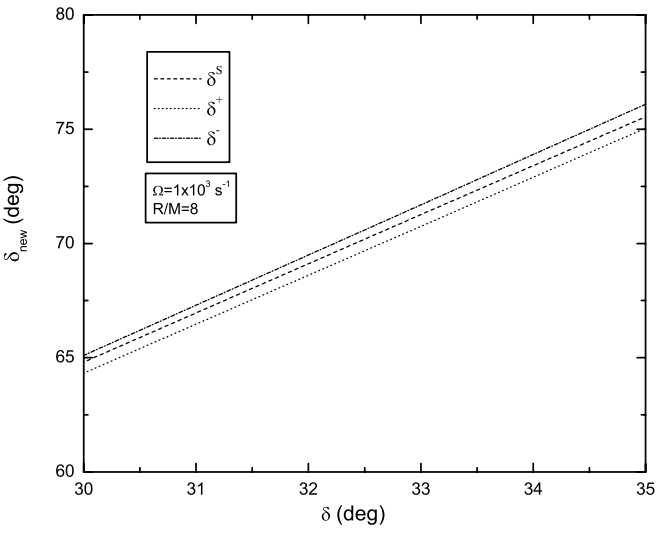

FIG. 10.—Effect of frame dragging on the photon trajectory; $\delta^{\rm S}$ illustrates the deflection in Schwarzschild spacetime, and δ^+, δ^- illustrate the deflection in the tangentially backward direction and in the tangentially forward direction, respectively, at the rotational equator of a neutron star.

6.3. *X-Ray Light Curves*

We can generate light curves in the soft X-ray regime for different spot cases. According to Pechenick et al. (1983), the total energy flux observed is

$$F_{\rm X} = \sum I_0\left(\frac{R}{r_0}\right)^2 A\left(\theta_0; f, \frac{M}{R}, \alpha\right), \tag{42}$$

where I_0 is the energy flux from each cell at the surface, including the factor of enhanced emission. We adopt $\delta_{\rm new}$ instead of $\delta_{\rm new}^{\rm S}$ to incorporate the asymmetry due to rotation. $\sum$ denotes the summation of the contribution from each cell. The comparisons of light curves with different rotational frequencies are made in Figures 11 and 12 with $R/M \sim 8$ and

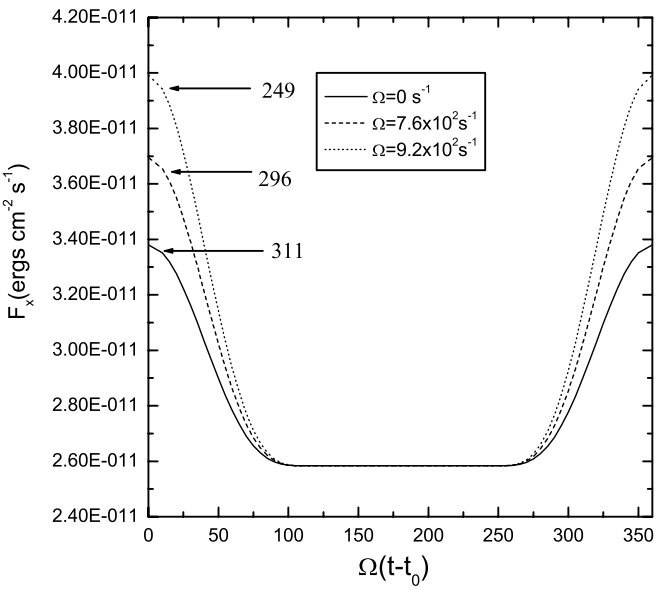

FIG. 11.—Thermal X-ray pulse profiles at the peak time for a neutron star with $R/M \sim 8$, $T_c = 10^7$ K, and $\Delta E = 10^{42}$ ergs at $\rho_{\rm glitch} = 10^{13}$ g cm^{-3} and $\theta = \phi = 90^\circ$ in an orientation with $\alpha = 3^\circ$, $f(\delta) = \cos\delta$, and $\beta = \gamma = 90^\circ$ for a spot case. Three cases with different rotational frequency are compared. The numbers associated with the arrows indicate the number of days after the glitch.

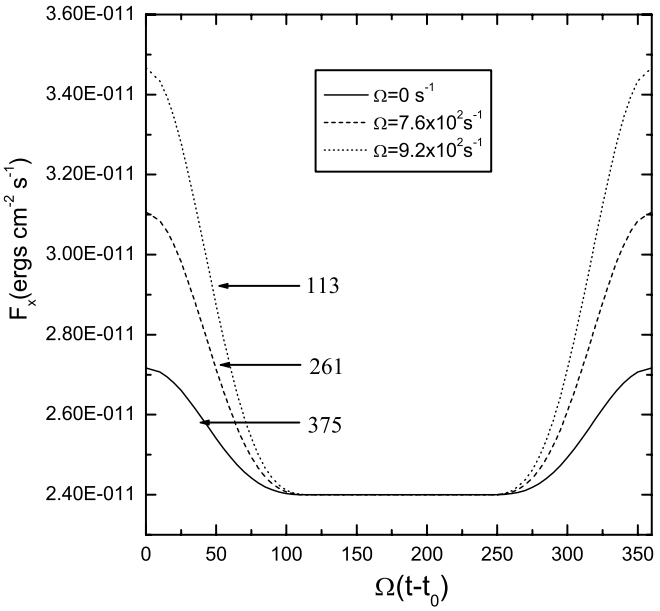

FIG. 12.—Same as Fig. 11, but with $R/M \sim 6$.

$R/M \sim 6$, respectively. We have not found any asymmetry in the pulse profile for the rotational cases.

7. CONCLUSION AND DISCUSSION

In this paper we have developed an anisotropic heat transport equation. This equation is then employed to simulate thermal afterglows resulting from pulsar glitches. We have examined the effects of rotation on the thermal responses. Although rotation does not have significant effect on the rate of standard cooling (Miralles et al. 1993), noticeable changes in duration and intensity of thermal afterglows are found in spot cases. In comparison with static cases, afterglows with shorter duration and larger intensity are found in rotating stars. These are not unexpected when the effects of centrifugal forces on the stellar structure as well as heat transport are realized. We suggest that rotation prompts a faster and larger response. In equation (A1) of the Appendix, the radial diffusion coefficient is given by $D_r = -C_2/C_6$, which contains the factors of the rotating metric and hence is a function of rotational frequency. D_r increases with rotational frequency (see Table 1) and prompts a faster response. On the other hand, the rotation also increases the distance that heat pulses need to travel in order to give an afterglow on the surface. The resultant effect on the duration and the magnitude of the thermal afterglow depends on the interplay between these two factors. We have also generated the thermal X-ray light curves for the spot cases. The effects of gravitational lensing and frame dragging are fully taken into account. Apart from the peak time and the peak intensity, we have not found any significant effect of rotation on the morphology of the pulse profile.

TABLE 1

DEVIATION OF RADIAL DIFFUSION COEFFICIENT

$R/M = 8$		$R/M = 6$	
Ω (s^{-1})	ΔD_r ($cm^2\ s^{-1}$)	Ω (s^{-1})	ΔD_r ($cm^2\ s^{-1}$)
152.....	14.1	200.....	28.6
305.....	56.3	300.....	60.3
500.....	152.2	513.....	183.0
579.....	201.3	586.....	238.0
762.....	344.6	760.....	395.8
839.....	416.1	802.....	418.2

NOTE.—Shown is the deviation of the radial diffusion coefficient from the nonrotational value (i.e., $\Delta D_r = D_{r,\Omega\neq 0} - D_{r,\Omega=0}$) at the location of energy deposition for spot cases (i.e., at $\rho_{\rm glitch} = 10^{13}$ g cm^{-3}, $\theta = \phi = 90^\circ$, with $\Delta E = 10^{42}$ ergs, $T_c = 10^7$ K) at $t = 0$ s as a function of rotational frequency.

Hirano et al. (1997) characterize the thermal afterglow by the fractional increase of surface temperature at the peak and the peak time. They also propose a framework to set constraints on the equation of state by using these two parameters. Since the peak time is larger and the amplitude is smaller for a stiff star than for a soft star, without taking the effects of rotation into consideration we may underestimate the stiffness of the equation of state.

One of the practical questions is the detectability of these soft X-ray transients, which depends on the sensitivity of the detector. For the spot cases considered in this paper, the glitch events are able to be detected by state-of-the-art X-ray satellites such as *XMM-Newton*. Once the observational data of these thermal afterglows are obtained, these can be used in putting constraints on the equation of state of neutron stars as well as the glitch models by the method of periodic analysis (Andersen & Ögelman 1997).

In our calculations, we have neglected interstellar absorption, magnetospheric effects, magnetic field effect (Page 1995), and the possibility of uplifting and local expansion of matter caused by heat deposition (Eichler & Cheng 1989). We would like to remark that we have ignored the contribution of impurity scattering in the thermal conductivity, which may be important when $T \leq 10^7$ (Yakovlev & Urpin 1980). We have also assumed that no other glitch events occur during the evolution of the afterglow. Glitch events occurring too frequently may result in a pileup of pulses, as well as a long-term variation of the total thermal radiation, which would eventually reduce the detectability of the thermal afterglow (Li 1997). Moreover, we keep a constant rotational frequency during the evolution of the afterglow. However, glitches recover exponentially and hence Ω should vary with time. Also, the effects should be more important for fast rotation; a fully numerical scheme is needed to calculate the metric in the fast-rotation case. For further study, all these effects have to be taken into account.

APPENDIX

The anisotropic relativistic heat transport equation (i.e., eq. [28]) can be rearranged into a standard form of partial differential equation as follows:

$$0 = C_1\frac{\partial^2 T}{\partial t^2} + C_2\frac{\partial^2 T}{\partial r^2} + C_3\frac{\partial^2 T}{\partial \theta^2} + C_4\frac{\partial^2 T}{\partial \phi^2} + C_5\frac{\partial^2 T}{\partial t\partial \phi} + C_6\frac{\partial T}{\partial t} + C_7\frac{\partial T}{\partial r} + C_8\frac{\partial T}{\partial \theta} + C_9\frac{\partial T}{\partial \phi} + C_{10}T + C_{11}. \quad \text{(A1)}$$

The expressions of coefficients C_1 through C_{11} are listed as follows (with $G = c = 1$):

$$C_1 = 2u^t K(g^{tt} - u^t u^t), \tag{A2}$$

$$C_2 = u^t K g^{rr}, \tag{A3}$$

$$C_3 = u^t K g^{\theta\theta}, \tag{A4}$$

$$C_4 = K\left[u^t\left(g^{\phi\phi} - u^\phi u^\phi\right) + u^\phi\left(g^{t\phi} - u^t u^\phi\right)\right], \tag{A5}$$

$$C_5 = K\left[3u^t\left(g^{t\phi} - u^\phi u^t\right) + u^\phi(g^{tt} - u^t u^t)\right], \tag{A6}$$

$$C_6 = \frac{\partial K}{\partial \phi}\left[u^t\left(g^{t\phi} - u^\phi u^t\right) + u^\phi(g^{tt} - u^t u^t)\right] + C_v\left[\frac{dP}{d\rho}(u^t u^t - g^{tt}) + u^t u^t\right], \tag{A7}$$

$$C_7 = K\frac{\partial u^t}{\partial r}g^{rr} + u^t\frac{\partial K}{\partial r}g^{rr} + u^t K\frac{\partial g^{rr}}{\partial r} + \left(3\Gamma^t_{rt} + \frac{\partial \lambda}{\partial r} + \Gamma^\theta_{r\theta} + \Gamma^\phi_{r\phi}\right)u^t K g^{rr} + 2\Gamma^t_{r\phi}u^\phi K g^{rr} - u^t K g^{rr} a_r, \tag{A8}$$

$$C_8 = K\frac{\partial u^t}{\partial \theta}g^{\theta\theta} + u^t\frac{\partial K}{\partial \theta}g^{\theta\theta} + u^t K\frac{\partial g^{\theta\theta}}{\partial \theta} + \left(3\Gamma^t_{\theta t} + \frac{\partial \lambda}{\partial \theta} + \Gamma^\theta_{\theta\theta} + \Gamma^\phi_{\theta\phi}\right)u^t K g^{\theta\theta} - u^t K g^{\theta\theta} a_\theta, \tag{A9}$$

$$C_9 = \frac{\partial K}{\partial \phi}\left[u^t\left(g^{\phi\phi} - u^\phi u^\phi\right) + u^\phi\left(g^{t\phi} - u^t u^\phi\right)\right], \tag{A10}$$

$$C_{10} = -\left[a_r(C_7 + u^t K g^{rr} a_r) + a_\theta\left(C_8 + u^t K g^{\theta\theta} a_\theta\right) + u^t K g^{rr}\frac{\partial a_r}{\partial r} + u^t K g^{\theta\theta}\frac{\partial a_\theta}{\partial \theta}\right], \tag{A11}$$

$$C_{11} = \frac{Q_\nu}{u^t}\left[\frac{dP}{d\rho}(u^t u^t - g^{tt}) + u^t u^t\right]. \tag{A12}$$

REFERENCES

Abramowicz, M. 1990, MNRAS, 245, 733
Abramowicz, M., Carter, B., & Lasota, J. P. 1988, Gen. Relativ. Gravitation, 20, 1173
Abramowicz, M., Miller, J., & Stuchlík, Z. 1993, Phys. Rev. D, 47, 1140
Abramowicz, M., & Prasanna, A. 1990, MNRAS, 245, 720
Alpar, M. A., Anderson, P. W., Pines, D., & Shaham, J. 1984, ApJ, 276, 325
Andersen, D. R., & Ögelman, H. 1997, ApJ, 475, 300
Anderson, P. W., & Itoh, N. 1975, Nature, 256, 25
Baym, G., & Pines, D. 1971, Ann. Phys., 66, 816
Carter, B., Langlois, D., & Sedrakian, D. M. 2000, A&A, 361, 795
Chandrasekhar, S., & Miller, J. 1974, MNRAS, 167, 63
Cheng, K. S., Alpar, M. A., Pines, D., & Shaham, J. 1988, ApJ, 330, 835
Cheng, K. S., Li, Y., & Suen, W. M. 1998, ApJ, 499, L45
Chong, N., & Cheng, K. S. 1994, ApJ, 425, 210
Eichler, D., & Cheng, A. F. 1989, ApJ, 336, 360
Flowers, E. G., & Itoh, N. 1981, ApJ, 250, 750
Freire, P. C., & da Costa, A. A. 1999, MNRAS, 304, 235
Gudmundsson, E. H., Pethick, C. J., & Epstein, R. I. 1983, ApJ, 272, 286
Hartle, J. B. 1967, ApJ, 150, 1005
Hartle, J. B., & Thorne, K. S. 1968, ApJ, 153, 807
Helfand, D. J., Gotthelf, E. V., & Halpern, J. P. 2001, ApJ, 556, 380
Hirano, S., Shibazaki, N., Umeda, H., & Nomota, K. 1997, ApJ, 491, 286
Hobbs, G., et al. 2002, MNRAS, 333, L7
Kapoor, R. C., & Datta, B. 1985, ApJ, 297, 413
Krawczyk, A., Lyne, A. G., Gil, J. A., & Joshi, B. C. 2003, MNRAS, 340, 1087
Larson, M. B., & Link, B. 2002, MNRAS, 333, 613
Li, Y. 1997, M.A. thesis, Univ. Hong Kong
Link, B., & Epstein, R. I. 1996, ApJ, 457, 844
Lyne, A. G., Shemar, S. L., & Smith, F. G. 2000, MNRAS, 315, 534
MacKeown, P. K. 1997, Stochastic Simulation in Physics (Singapore: Springer)
Maxwell, O. V. 1979, ApJ, 231, 201
Miralles, J. A., Van Riper, K. A., & Lattimer, J. M. 1993, ApJ, 407, 687
Page, D. 1995, ApJ, 442, 273
Pandharipande, V. 1971, Nucl. Phys. A, 174, 641
Pechenick, K. R., Ftaclas, C., & Cohen, J. M. 1983, ApJ, 274, 846
Ruderman, M. 1969, Nature, 223, 597
Shibazaki, N., & Lamb, F. K. 1989, ApJ, 346, 808
Tang, P. S., & Cheng, K. S. 2001, ApJ, 549, 1039
Tolman, R. C. 1934, Relativity, Thermodynamics, and Cosmology (Oxford: Clarendon)
Van Riper, K. A., Epstein, R. I., & Miller, G. S. 1991, ApJ, 381, L47
Wang, N., Manchester, R. N., Pace, R. T., Bailes, M., Kaspi, V. M., Stappers, B. W., & Lyne, A. G. 2000, MNRAS, 317, 843
Yakovlev, D. G., & Urpin, V. A. 1980, Soviet Astron., 24, 303
Zel'dovich, Ya. B., & Novikov, I. D. 1971, Relativistic Astrophysics, Vol. 1 (Chicago: Univ. Chicago Press)